WHOLE GENOME SEQUENCING REVEALS NOVEL MUTATIONS CAUSING AUTOSOMAL DOMINANT INHERITED MACULAR DEGENERATION

Shyamanga Borooah,[1,2,3] Chloe M. Stanton,[4] Joseph Marsh,[4] Keren J. Carss,[5,6] Naushin Waseem,[8] Pooja Biswas,[3] Georgios Agorogiannis,[1] Lucy Raymond,[6,9] Gavin Arno,[1,8] Andrew R.Webster[1,8]

[1]Moorfields Eye Hospital, London, UK
[2]Centre for Clinical Brain Sciences, School of Clinical Sciences, University of Edinburgh, Edinburgh, UK
[3]Shiley Eye Institute, University of California, San Diego, La Jolla, CA, USA
[4]Medical Research Council Human Genetics Unit, Medical Research Council Institute of Genetics and Molecular Medicine, University of Edinburgh, Edinburgh, UK
[5]Department of Hematology, University of Cambridge, Cambridge, UK
[6]NIHR BioResource - rare diseases, Cambridge University Hospitals NHS Foundation Trust, Cambridge Biomedical Campus, Cambridge, UK
[7]Department of Medical Genetics, University of Cambridge, Cambridge, United Kingdom.
[8]Institute of Ophthalmology, University College London, London, UK.

Author for correspondence:

Dr Shyamanga Borooah,
Shiley Eye Institute,
9415 Campus Point Drive,
San Diego, CA 92093

Phone: +1 (858) 405 2316
Email: shyamanga@aol.com

Abstract

Background Age-related macular degeneration (AMD) is a common sight threatening condition. However, there are a number of monogenic macular dystrophies that are clinically similar to AMD, which can potentially provide pathogenetic insights.

Methods Three siblings from a non-consanguineous Greek-Cypriot family reported central visual disturbance and nyctalopia. The patients had full ophthalmic examinations and color fundus photography, spectral- domain ocular coherence tomography and scanning laser ophthalmoscopy. Targeted polymerase chain reaction (PCR) was performed as first step to attempt to identify suspected mutations in *C1QTNF5* and *TIMP3* followed by whole genome sequencing.

Results The three patients were noted to have symptoms of nyctalopia, early paracentral visual field loss and, in older patients, central vision loss. Imaging identified pseudodrusen, retinal atrophy and RPE-Bruch's membrane separation. Whole genome sequencing of the proband revealed two novel heterozygous variants in *C1QTNF5,* c.556C>T and c.569C>G. The mutation segregated with disease in this family, occurred in *cis*, and resulted in missense amino acid changes P186S and S190W in C1QTNF5. *In silico* modelling of the variants revealed that the S190W mutations was likely to have the greatest pathologic effect and that the combination of the mutations was likely to have an additive effect.

Conclusions The novel mutations in *C1QTNF5* identified here expand the genotypic spectrum of mutations causing late-onset retinal dystrophy.

Keywords: Macular dystrophy, nyctalopia, whole genome sequencing, *C1QTNF5*,

WHOLE GENOME SEQUENCING REVEALS NOVEL MUTATIONS CAUSING AUTOSOMAL DOMINANT INHERITED MACULAR DEGENERATION

Introduction

Age-related macular degeneration (AMD) is one of the commonest causes of blindness in the developed world (1). Early AMD is identified clinically by focal sub-retinal deposits known as drusen (2). Late stage disease results in two main forms of disease; neovascular or wet AMD which results from choroidal neovascularization and dry or non-neovascular AMD which results in an insidious loss of the retinal pigment epithelium (RPE) followed by neuro-retinal atrophy leading to geographic atrophy. Non-nvAMD is the commonest form of AMD accounting for up to 90% of cases (3).

There are a number of Mendelian inherited diseases which mimic AMD with the development of drusen or drusen-like sub-RPE deposits, pseudodrusen, retinal atrophy and choroidal neovascularization (CNV). These diseases include late-onset retinal dystrophy (L-ORD), Sorsby fundus dystrophy (SFD) and dominant drusen/Doyne's honeycomb macular dystrophy (DD) for which a number of mutations have previously been described (4-6).

In this article we describe the investigation of members of a family who present with macular degeneration with an autosomal dominant inheritance pattern. Standard screening of known mutation loci was negative for disease in this family.

Materials and Methods

Three patients from a single family were examined in the clinics of Moorfields eye hospital (MEH), London. All subjects underwent an ophthalmic examination performed by an ophthalmologist, which included best-corrected Snellen visual acuity (BCVA), slit lamp biomicroscopy of the anterior segment, and dilated fundus examination. Color fundus photographs were obtained (Topcon 3D OCT, Topcon Corporation, Tokyo, Japan). Fundus autofluorescence (FAF) imaging was performed using 30° or 55° lenses using a confocal

scanning laser ophthalmoscope (HRA+OCT Spectralis, Heidelberg Engineering, Heidelberg, Germany) and spectral-domain optical coherence tomography (SD-OCT) (HRA+OCT Spectralis, Heidelberg Engineering, Heidelberg, Germany) were performed on all patients. Additional pseudo color and ultra-widefield confocal scanning laser (Optos plc, Dunfermline, UK) were performed on some patients. Full-field electroretinography (ffERG) and pattern ERG (PERG) were also performed according to the standards agreed by the International Society for Clinical Electrophysiology of Vision Standards on one of the patients (7, 8). Patients were dark adapted for a minimum of 20 minutes. The ffERGs were recorded under dark-adapted conditions to flash strengths of 0.01 and 10.0 candelas/s/m^{-2} (cd/s/m^{-2}) and light-adapted ffERGs to a flash strength of 3.0 cd/s/m^{-2} (30 Hz and 2 Hz). Informed written consent and peripheral blood samples were obtained for genetic analysis from all participants according to the protocols approved by the Research Management Committees of Moorfields Eye Hospital and in agreement with the tenets of the declaration of Helsinki.
For initial molecular investigations in the proband a PCR amplification was performed to amplify intron 4 and exon 5 of *TIMP3* and the c.489 C>G mutation region in *C1QTNF5*. The amplicons were sequenced using standardized sequencing protocols. Whole genome sequencing was performed as part of the National Institute for Health Research (NIHR) BioResource- Rare Diseases study and was performed as previously described (9). Briefly, WGS used the Illumina TruSeq DNA PCR-Free Sample preparation kit (Illumina, Inc.) and sequenced using an Illumina HiSeq 2500, generating minimum coverage of 15× for approximately 95% of the genome. Reads were aligned to the Genome Reference Consortium human genome build 37 (GRCh37) using Isaac Genome Alignment Software (version 01.14; Illumina, Inc.). Single nucleotide variations and small insertion deletions were identified using Isaac Variant Caller (version 2.0.17). To facilitate variant interpretation, a list of reported IRD-associated genes was assembled, including genes associated with syndromic

forms of IRD or albinism, from various sources including RetNet and literature searches. This list was manually curated according to published evidence of pathogenicity to compile a shortlist of 224 high-confidence IRD associated genes. To identify pathogenic variants, a two-step variant filtering protocol was designed, utilizing automated filtering followed by manual review. For SNVs and indels, automated filtering identified variants that fulfil the following criteria: passes standard Illumina quality filters in >80% of the whole NIHR BioResource Rare Diseases cohort (n. 6,688); predicted to be a high impact, medium impact, or splice region variant, or present in the HGMD Pro database; 22 and has minor allele frequency (MAF) < 0.01 in control datasets including the NIHR BioResource Rare Diseases cohort and the Exome Aggregation Consortium (ExAC) database. If a variant is present in the HGMD Pro database, a higher MAF threshold of 0.1 was used. Finally, we identified just those variants that affect an IRD-associated gene. Confirmatory bidirectional Sanger sequencing of *C1QTNF5* was performed in all available family members. Amplification of DNA was performed using specifically designed primers by polymerase chain reaction, and the resulting fragments were sequenced using standard protocols.

Variant nomenclature was assigned in accordance with GenBank Accession number NM_015645.4, with nucleotide position 1 corresponding to the A of the ATG initiation codon. Variants were identified as novel if not previously reported in the literature and if absent from dbSNP (http://www.ncbi.nlm.nih.gov/projects/SNP/), EVS, and the Exome Aggregation Consortium database (ExAC; http://exac.broadinstitute.org) containing 61 486 exomes, all accessed on 25/3/2016. Where relevant, potential splice site disruption was assessed using Splice Site Prediction by Neural Network (http://www.fruitfly.org/seq_tools/splice.html).

UCSC genome browser was used to check for orthologues and conservation of protein sequence amongst species. Pathogenicity of the novel variant and original mutations were

assessed using predictive algorithms of "Sorting Intolerant From Tolerant" (SIFT; in the public domain, http://sift.jcvi.org), Polymorphism Phenotyping v2 (PolyPhen-2; in the public domain, http://genetics.bwh.harvard.edu/pph2) and Mutationtaster (http://www.mutationtaster.org/).

The effects of each amino acid substitution on protein folding and assembly were predicted with the FoldX package, using the homotrimeric crystal structure of the human C1QTNF5 gC1q domain (PDB ID: 4NN0). A model of the 18-mer assembly was constructed based upon contacts present in the asymmetric unit of this structure. The predicted effect upon on protein folding was calculated using from the FoldX-calculated change in stability induced by an amino acid substitution for the isolated monomeric subunit. The predicted effect on trimer assembly was calculated as the difference between the change in stability for the trimer and the monomeric subunit in isolation. Finally, the predicted effect on higher-order assembly was calculated as the difference between the change in stability for the 18-mer and the trimer. When considering the trimer and 18-mer complexes, only a single subunit was mutated, reflecting the heterozygous nature of the mutations. The FoldX "RepairPDB" function was run prior to mutations. Ten FoldX replicates were performed for each mutation, and the average was presented here.

Results

A three generation non-consanguineous Greek Cypriot family with macular degeneration was studied. Inheritance followed an autosomal dominant pattern (Fig 1A). The proband (II:4) was initially seen in 2011 aged 65. He was already registered blind and was otherwise well except for cardiovascular disease for which he had been treated with a stent 4 years previously. He continued to take aspirin, atenolol, clopidogrel, simvastatin and famotidine. He was asymptomatic until his sixth decade. Aged 54 years he presented with difficulty with

night time vision, driving and reading. By the time of examination at MEH his BCVA was hand movements bilaterally. Slit lamp examination revealed posterior chamber intra-ocular lenses bilaterally (Fig 2A). Fundus examination identified widespread retinal atrophy in the macula within the arcades with further peripheral scalloped atrophy (Fig 2B and C). SD-OCT with a cross section at the fovea revealed marked central retinal thinning suggesting neuroretinal atrophy at the fovea, sub-RPE deposits temporally and a thinned choroid (Fig 2D and E). Visual field to confrontation was diminished. Known mutations for L-ORD and SFD were excluded by PCR based sequencing.

The sister of the proband (II:3) was first seen aged 67. She had experienced 4 years of night blindness with worsening of central vision in both eyes and had a previous medical history of treated hypertension, asthma and ischemic heart disease. Examination revealed a BCVA of 6/12 bilaterally. Anterior segment examination revealed mild cataracts with only a few long anterior zonules superiorly which were difficult to identify on photography but were more clearly seen on examination (Fig 3A). Fundus examination at first presentation showed marked atrophy at the macula with foveal sparing (Fig 3B) and more scalloped atrophy to the mid-periphery which were clear on SLO (Fig 3C). SD-OCT revealed near uniform sub-retinal thickening across the fundus (Figs 3D, 3E). Goldmann visual field (supplementary figure 1) were markedly reduced using III4e target and after 5 years of review there was marked progression of macular changes (Fig 3D). The phenotype resembled late-onset retinal dystrophy (L-ORD) which is an autosomal dominant retinal dystrophy usually presenting with dark adaptation delay and later central visual loss and which demonstrates marked macular, retinal atrophy and sub-RPE thickening on SD-OCT. However, testing for the c.489 C>G, p.S163R mutation for L-ORD did not identify any pathogenic change.

Case (II:7) was first seen in 2014 aged 54. She complained of mild dark adaptation delay. She was myopic with a previous history of right anisometropic amblyopia. She was otherwise

healthy except for a history of hypertension controlled with losartan. Her BCVA was 6/18 right and 6/5 left. Examination revealed fine long anterior zonule fibers superiorly at the lens (Fig 4A). Fundus examination revealed small white lesions outside the arcades with atrophy temporal to the macula (Fig 4B). There was bilateral peripapillary atrophy greater on the right than the left eye. Occasional pigment clumps were seen. The SD-OCT revealed areas of sub-retinal thickening. This was again in the temporal peripheral macula consistent with other L-ORD cases and this region was also the first to have reduced auto-fluorescence (Figs 4C, D and E). Ishihara color vision testing was full. Humphrey visual field testing identified increased blind spots on the right greater than the left (supplementary figure 2). Electroretinography showed mild generalized loss of rod function with no cone system involvement.

The absence of causative mutations at the suspected loci for SFD and L-ORD prompted investigation using whole genome sequencing. The proband was found to have two heterozygous variants at c.556C>T (p.P186S) and c.569C>G (p.S190W) in *C1QTNF5* (chromosome 11 position 119210217 and 119210204 respectively). These appeared to be in *cis* from inspection of the WGS reads (supplementary figure 4) in which the variants were always on the same read, when spanning both loci. These were confirmed by bidirectional sequencing of the PCR product of primers flanking this region (Fig 1B), and were shown to segregate with the disorder in two further affected and 3 unaffected siblings (likelihood given no linkage = 1:32, p= 0.03, LOD score = 1.5)

To see if the two variants were novel we reviewed the ExAC database. The amino acids are highly evolutionarily conserved across species (supplementary figure 3). To confirm that the variants were pathogenic we used several online prediction tools to assess the impact of the amino acid substitutions (Fig 5B). The amino acid substitution S190W was found to be more

consistently damaging than the P186S. The findings also compare favorably when compared to the prototypic S163R mutation suggesting that the variants are pathogenic.

To understand how the variants may potentially affect trimerization and multimers formation we performed *in silico* mutagenesis as previously described. (10)Computational modelling indicated that the S190W substitution had a highly destabilizing effect upon trimer assembly, resulting in a calculated free energy difference (ΔΔG) of 9.7 kcal/mol, compared to the wild-type protein (Fig 5B). When combined with P186S, there was an additive effect of both the mutations, with a total ΔΔG of 12.3 kcal/mol. This is as highly destabilizing as the known pathogenic variants S163R and G216C reported previously.(10) To identify if a potential mechanism for pathogenicity we generated a three dimensional model of monomeric and multimeric C1QTNF5. The novel variants P186S and S190W cluster near to previously identified pathogenic mutations on the surface of the globular domain of C1QTNF5 suggesting that this is an important region for C1QTNF5 multimerisation.

Discussion

This report describes three cases from a pedigree who present with macular dystrophy with an autosomal dominant inheritance pattern. Although the cases tested negative for the prototype S163R mutation in *C1QTNF5* which results in L-ORD, their clinical presentation was mainly consistent with L-ORD (11-17) as outlined by a previously described staging system (18). In this simple three stages system, stage 1 (0-40 years of age) patients were asymptomatic but may demonstrate long anterior zonules (LAZ). In stage 2 (40-60 years of age), patients report dark adaptation delay and nyctalopia and are noted to have macular degeneration sparing the fovea and clinical dark adaptometry delay. In stage 3 (>60 years of age), patients lose central vision progressively and by late stage 3 disease there is full visual field loss. The clinical findings of L-ORD have been summarized by a number of studies (11-17).

There were a number of differences in the affected patients when compared to cases harboring the classical S163R mutations. The LAZ normally demonstrate peripupillary trans-illumination defects however these were absent in all our cases. Additionally, the proband (II:4) already had bilateral cataract surgery which would have precluded the identification of long anterior zonules (Fig 2A). There was some variability in the presentation of visual symptoms amongst the cases. All three patients admitted to having symptoms of dark adaptation delay. However, proband (II:4) and (II:7) described symptoms from the age of 54. However, case (II:3) appears to have milder disease with symptoms starting in her early seventh decade. Similarly case (II:3) has conserved central vision whilst proband (II:4) who is younger has already lost central vision bilaterally.

L-ORD is a fully penetrant autosomal dominant macular and retinal degeneration. The first identified mutation in *C1QTNF5* resulted from a substitution (S163R) (L-ORD, OMIM 608752). However, recently several additional pathogenic variants in *C1QTNF5* have been identified (10). Patients with L-ORD develop early drusenoid deposits, thick sub-RPE deposits which extend to the *ora serrata*, RPE atrophy and later widespread geographic atrophy (15). L-ORD results from a mutation in the gene *C1QTNF5* (6). The gene encodes a protein of the same name which is expressed by the RPE and ciliary body within the eye and is composed of a globular domain and collagen like domain with a nitrile end (19). The protein belongs to the C1Q tumor necrosis superfamily which includes adiponectin (20). C1QTNF5 has been shown to have metabolic function increasing AMPK phosphorylation (21).

C1QTNF5 is composed of 3 exons. Exon 1 is a non-coding exon. Exon 2 contains the start codon for translation codes for the N-terminal signal peptide and the collagen-like domain and exon 3 codes for the C-terminal globular domain (22). Translation results in a 25kDa monomeric protein. C1QTNF5 forms trimers and has been shown to form high order

multimers (6, 14, 19). The proposed novel pathogenic variants in this pedigree are located at c.556C>T (P186S) and c.569C>G (S190W) in *C1QTNF5*.

The exact effect of the mutations on C1QTNF5 protein are yet to be established. The crystal structure of full length C1QTNF5 was demonstrated by Tu and Palczewski (19). C1QTNF5 has a complex structure leading to the formation of high order multimers resulting from complex hydrophobic and hydrophilic interactions, hydrogen bonds and disulfide bonds (19, 23). The globular domain, where the mutations are all located, appears important for trimerization of C1QTNF5. The globular heads of C1QTNF5 contain 10 strands arranged in two anti-parallel β-sheets (24). The β-sheets are brought together by a hydrophobic 'zipper' (19).

The pathogenic variants identified in this study as well as the previously identified variants all encode amino acids found on the surface of the globular domain of C1QTNF5 (Fig 5A) and form part of an apical loop which is predicted to play an important role in the interaction between C1QTNF5 monomers (19). As a result it is predicted that they may disrupt trimerization. Using *in silico* modelling and energy stability calculations both novel variants were found to destabilize C1QTNF5 folding. A combination of both variants may result in a greater pathogenic impact on C1QTNF5 stability. A review of the GNOMAD database reveals that there are loss of function variants in *C1QTNF5*, which do not result in eye disease suggesting that the changes are not likely to be due haplodeficiency. Therefore, the two variants are likely to be dominant negative or neomorphic alleles if they are pathogenic. As the mutations were found in *cis* it was not thought predicted that disease severity would be altered by the two mutations with a dominant-negative mechanism proposed. The onset and progression of the case phenotypes was within the normal range of expected phenotypes for L-ORD.

Recent studies using a human RPE expressing the recently identified mutations appear to confirm *in silico* predictions. There was a change in the polarity of C1QTNF5 secretion from the apical to basal membranes of RPE. This may contribute to the thick deposits seen in post-mortem samples of human L-ORD eyes and in the BM-RPE separation noted in the retinal SD-OCT scans of our patients (10, 15, 17, 25). We propose a similar disease mechanism for the novel pathogenic variants identified in our patients.

A problem has been the validation of candidate pathogenic variants. Whilst functional studies have so far proved the gold standard for validation it is currently too time consuming and costly to provide a functional characterization of all newly discovered candidate pathogenic variants. A set of online tools has proven useful to confirm pathogenicity as has been used in this study. We also describe the use of computer modelling to identify protein stability. Analysis comparing the accuracy of modelling tools compared to functional and experimental studies has shown that although they are accurate in identifying energy stability changes, they underestimate the ΔΔG (26). However, modelling tools may be particularly useful to test in the setting of genes coding for proteins involved in complex or high order structures such as C1QTNF5 where generation of complexes or high order hetero-multimers may be difficult *in vitro.* Tools which combine various predictions including computer modelling such as meta-predictors are increasingly being developed using machine learning and may prove even more accurate in prediction in the future (27).

In summary, we describe the clinical and molecular findings of a family presenting with a dominant macular degeneration. We identified novel pathogenic variants in the gene *C1QTNF5* which resulted in the clinical findings of nyctalopia, thick sub–RPE deposits, pseudodrusen, RPE and neuro-retinal atrophy. The condition shares clinical similarities with the autosomal dominant macular degeneration L-ORD.

Acknowledgements

We thank Dr David Goodsell, Scripps research institute for advice regarding protein modelling.

Disclosure statement

All authors have completed the ICMJE uniform disclosure form at www.icmje.org/coi_disclosure.pdf and declare: no support from any organization for the submitted work; no financial relationships with any organizations that might have an interest in the submitted work in the previous three years; no other relationships or activities that could appear to have influenced the submitted work.

Funding

This work was supported by The National Institute for Health Research England (NIHR) for the NIHR BioResource – Rare Diseases project (grant number RG65966); The work was also supported by the Moorfields Eye Hospital, UCL Institute of Ophthalmology NIHR Biomedical Research Centre; Shyamanga Borooah was supported by a Fulbright-Fight for Sight scholarship and a Foundation Fighting Blindness Career Development Award; Joe Marsh was supported by a MRC Career Development Award (MR/M02122X/1); Gavin Arno was sponsored by a Fight for Sight senior research fellowship.

References

1. Bourne RR, Jonas JB, Flaxman SR, Keeffe J, Leasher J, Naidoo K, et al. Prevalence and causes of vision loss in high-income countries and in Eastern and Central Europe: 1990-2010. Br J Ophthalmol. 2014;98(5):629-38.

2. Davis MD, Gangnon RE, Lee LY, Hubbard LD, Klein BE, Klein R, et al. The Age-Related Eye Disease Study severity scale for age-related macular degeneration: AREDS Report No. 17. Arch Ophthalmol. 2005;123(11):1484-98.

3. Klein R, Klein BE, Linton KL. Prevalence of age-related maculopathy. The Beaver Dam Eye Study. Ophthalmology. 1992;99(6):933-43.

4. Stone EM, Lotery AJ, Munier FL, Heon E, Piguet B, Guymer RH, et al. A single EFEMP1 mutation associated with both Malattia Leventinese and Doyne honeycomb retinal dystrophy. Nat Genet. 1999;22(2):199-202.

5. Weber BH, Vogt G, Pruett RC, Stohr H, Felbor U. Mutations in the tissue inhibitor of metalloproteinases-3 (TIMP3) in patients with Sorsby's fundus dystrophy. Nat Genet. 1994;8(4):352-6.

6. Hayward C, Shu X, Cideciyan AV, Lennon A, Barran P, Zareparsi S, et al. Mutation in a short-chain collagen gene, CTRP5, results in extracellular deposit formation in late-onset retinal degeneration: a genetic model for age-related macular degeneration. Hum Mol Genet. 2003;12(20):2657-67.

7. McCulloch DL, Marmor MF, Brigell MG, Hamilton R, Holder GE, Tzekov R, et al. ISCEV Standard for full-field clinical electroretinography (2015 update). Doc Ophthalmol. 2015;130(1):1-12.

8. Bach M, Brigell MG, Hawlina M, Holder GE, Johnson MA, McCulloch DL, et al. ISCEV standard for clinical pattern electroretinography (PERG): 2012 update. Doc Ophthalmol. 2013;126(1):1-7.

9. Carss KJ, Arno G, Erwood M, Stephens J, Sanchis-Juan A, Hull S, et al. Comprehensive Rare Variant Analysis via Whole-Genome Sequencing to Determine the Molecular Pathology of Inherited Retinal Disease. Am J Hum Genet. 2017;100(1):75-90.

10. Stanton CM, Borooah S, Drake C, Marsh JA, Campbell S, Lennon A, et al. Novel pathogenic mutations in C1QTNF5 support a dominant negative disease mechanism in late-onset retinal degeneration. Sci Rep. 2017;7(1):12147.

11. Jacobson SG, Cideciyan AV, Wright E, Wright AF. Phenotypic marker for early disease detection in dominant late-onset retinal degeneration. Invest Ophthalmol Vis Sci. 2001;42(8):1882-90.

12. Soumplis V, Sergouniotis PI, Robson AG, Michaelides M, Moore AT, Holder GE, et al. Phenotypic findings in C1QTNF5 retinopathy (late-onset retinal degeneration). Acta Ophthalmol. 2013;91(3):e191-5.

13. Vincent A, Munier FL, Vandenhoven CC, Wright T, Westall CA, Heon E. The characterization of retinal phenotype in a family with C1QTNF5-related late-onset retinal degeneration. Retina. 2012;32(8):1643-51.

14. Mandal MN, Vasireddy V, Reddy GB, Wang X, Moroi SE, Pattnaik BR, et al. CTRP5 is a membrane-associated and secretory protein in the RPE and ciliary body and the S163R mutation of CTRP5 impairs its secretion. Invest Ophthalmol Vis Sci. 2006;47(12):5505-13.

15. Kuntz CA, Jacobson SG, Cideciyan AV, Li ZY, Stone EM, Possin D, et al. Sub-retinal pigment epithelial deposits in a dominant late-onset retinal degeneration. Invest Ophthalmol Vis Sci. 1996;37(9):1772-82.

16. Cukras C, Flamendorf J, Wong WT, Ayyagari R, Cunningham D, Sieving PA. Longitudinal Structural Changes in Late-Onset Retinal Degeneration. Retina. 2016;36(12):2348-56.

17. Duvall J, McKechnie NM, Lee WR, Rothery S, Marshall J. Extensive subretinal pigment epithelial deposit in two brothers suffering from dominant retinitis pigmentosa. A histopathological study. Graefes Arch Clin Exp Ophthalmol. 1986;224(3):299-309.

18. Borooah S, Collins C, Wright A, Dhillon B. Late-onset retinal macular degeneration: clinical insights into an inherited retinal degeneration. Br J Ophthalmol. 2009;93(3):284-9.

19. Tu X, Palczewski K. The macular degeneration-linked C1QTNF5 (S163) mutation causes higher-order structural rearrangements. J Struct Biol. 2014;186(1):86-94.

20. Ressl S, Vu BK, Vivona S, Martinelli DC, Sudhof TC, Brunger AT. Structures of C1q-like proteins reveal unique features among the C1q/TNF superfamily. Structure. 2015;23(4):688-99.

21. Park SY, Choi JH, Ryu HS, Pak YK, Park KS, Lee HK, et al. C1q tumor necrosis factor alpha-related protein isoform 5 is increased in mitochondrial DNA-depleted myocytes and activates AMP-activated protein kinase. J Biol Chem. 2009;284(41):27780-9.

22. Chavali VR, Sommer JR, Petters RM, Ayyagari R. Identification of a promoter for the human C1Q-tumor necrosis factor-related protein-5 gene associated with late-onset retinal degeneration. Invest Ophthalmol Vis Sci. 2010;51(11):5499-507.

23. Wong GW, Krawczyk SA, Kitidis-Mitrokostas C, Revett T, Gimeno R, Lodish HF. Molecular, biochemical and functional characterizations of C1q/TNF family members: adipose-tissue-selective expression patterns, regulation by PPAR-gamma agonist, cysteine-mediated oligomerizations, combinatorial associations and metabolic functions. Biochem J. 2008;416(2):161-77.

24. Jones EY, Stuart DI, Walker NP. Structure of tumour necrosis factor. Nature. 1989;338(6212):225-8.

25. Milam AH, Curcio CA, Cideciyan AV, Saxena S, John SK, Kruth HS, et al. Dominant late-onset retinal degeneration with regional variation of sub-retinal pigment epithelium deposits, retinal function, and photoreceptor degeneration. Ophthalmology. 2000;107(12):2256-66.

26. Potapov V, Cohen M, Schreiber G. Assessing computational methods for predicting protein stability upon mutation: good on average but not in the details. Protein Eng Des Sel. 2009;22(9):553-60.

27. Tang H, Thomas PD. Tools for Predicting the Functional Impact of Nonsynonymous Genetic Variation. Genetics. 2016;203(2):635-47.

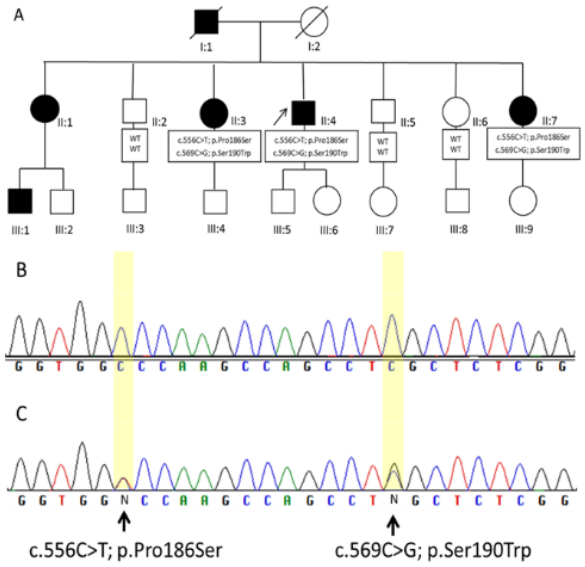

Figure 1

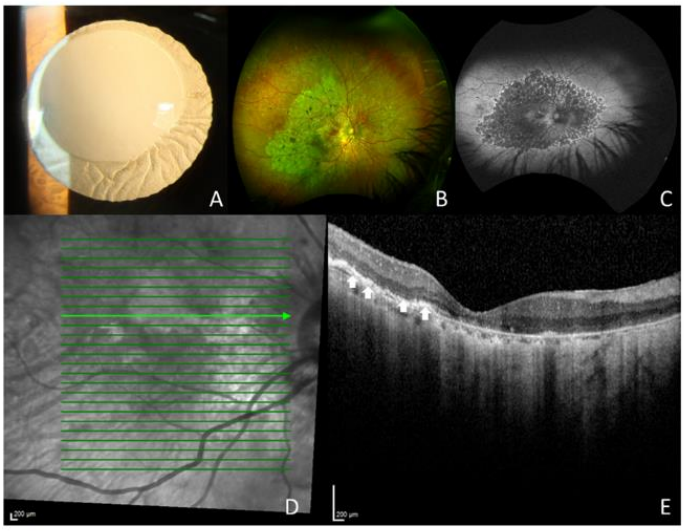

Figure 2

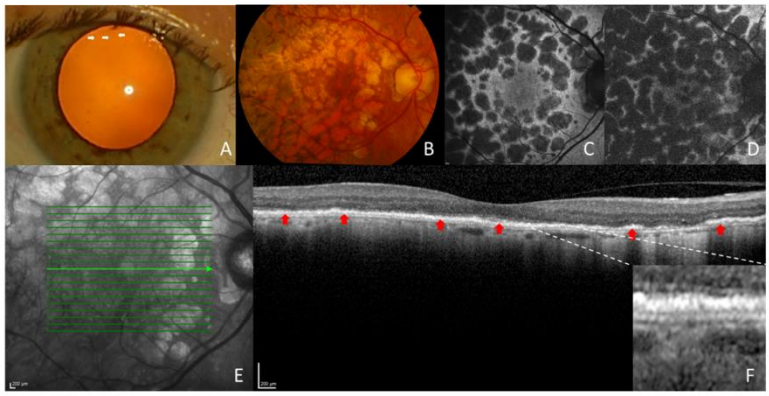

Figure 3

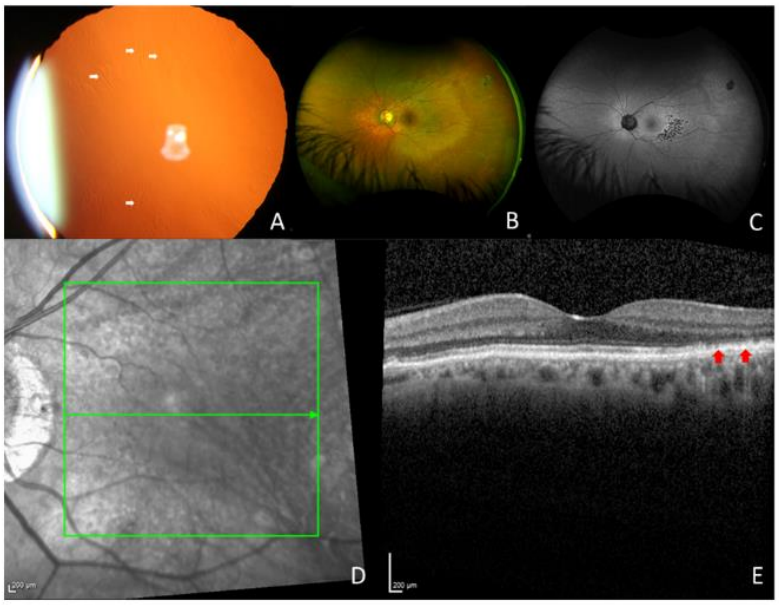

Figure 4

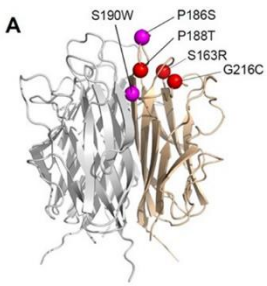

B

		Predicted destabilization, ΔΔG(kcal/mol)				Predicted impact of amino acid changes		
		Folding	Trimer assembly	High-order assembly	Total	PolyPhen	SIFT	Mutation Taster
Novel mutations	Pro186Ser	0.7	0.7	1.2	2.6	0.56 Tolerated	0.11 Benign	0.91 Disease causing
	Ser190Trp	-0.2	9.7	0.2	9.7	0.998 Probably damaging	0.03 Damaging	0.999 Disease causing
	Pro186Ser+ Ser190Trp	0.5	10.4	1.4	12.3			
Previously reported mutations	Ser163Arg	1.0	1.7	11.1	13.8	0.955 Possibly damaging	0.02 Damaging	0.91 Disease causing
	Pro188Thr	2.7	1.5	0.0	4.1	0.99 Probably damaging	0.25 Benign	0.88 Disease causing
	Gly216Cys	12.0	0.1	0.2	12.4	1.00 Probably damaging	0.00 Damaging	1.00 Disease causing

Figure 5

Figure Captions

Figure 1 Family pedigree and electropherograms for the affected family. (A) Inheritance followed an autosomal dominant inheritance pattern. Base pair status was confirmed at suspected mutation sites for individuals tested within the family. (B and C) Electropherograms depicting patient wild- type and mutation sequences from the sense strand of genomic DNA. (B) An unaffected sibling shows wild type sequence at the suspected mutation sites (yellow band) (C) The proband demonstrates substitutions c.556C>T (p.P186S) and c.569C>G (p.S190W) at the suspected sites (yellow band).

Figure 2 Imaging of proband (II:4). (**A**) Anterior segment photograph showing capsulorhexis and intra-ocular lens with no clear lens zonules. (**B**) Ultra-widefield pseudocolor images showing marked retinal atrophy involving the fovea and peripheral macula. (**C**) Ultra-widefield SLO showing marked scalloped areas of reduced autofluorescence surrounded by a ring of increased autofluorescence. (**D**) Infra-red line scan. (**E**) SD-OCT line scan through the fovea showing neuro-retinal atrophy and sub-retinal deposits (white arrows) above Bruch's membrane. Additionally there is a markedly atrophied choroid.

Figure 3 Imaging of case (II:3). (**A**) Anterior segment photograph showing sparse superior fine long anterior zonules (white arrows). (**B**) Color fundus photograph at initial presentation showing large islands of atrophy across the macula and beyond the vascular arcades but sparing the fovea. (**C**) SLO showing islands of reduced autofluorescence sparing the fovea at first presentation. (**D**) 5 years follow-up SLO showing increasing areas of reduced autofluorescence involving the fovea. (**E**) Infra-red line scan (**F**) SD-OCT line scan

performed at first presentation through the fovea showing mild neuro-retinal atrophy with loss of the ellipsoid and ELM hyper-reflective lines except for the fovea and sub-retinal deposits (red arrows) above Bruch's membrane (Inset). Additionally there is a markedly atrophied choroid.

Figure 4 Imaging of case (II:7). (**A**) Anterior segment photograph showing fine long anterior zonules superiorly and inferiorly. (**B**) Ultra-widefield pseudocolor images show mild peripapillary atrophy. Additionally there are pigmentary and atrophic changes in the temporal macula (**C**) Ultra-widefield SLO showing early scalloped areas of reduced autofluorescence surrounded by a ring of increased autofluorescence in the temporal macula. (**D**) Infra-red line scan. (**E**) SD-OCT line scan through the fovea showing loss of the ellipsoid and external limiting membrane in the temporal fovea with a sub-retinal deposit in the same region (red arrows).

Figure 5 C1QTNF5 protein structure model and stability prediction. (**A**) Transverse view of the three dimensional structure of trimeric C1QTNF5 with the positions of the previously described mutations (red) and novel mutations highlighted (purple). (**B**) Energy stability of the previous mutations and the new mutations as well as the combination of the two new variants in C1QTNF5 in monomer, trimer and high order.